Environmental Science: Atmospheres

ROYAL SOCIETY OF CHEMISTRY

PAPER

View Article Online
View Journal | View Issue

Cite this: *Environ. Sci.: Atmos.*, 2022, **2**, 1087

Furoyl peroxynitrate (fur-PAN), a product of VOC–NO_x photochemistry from biomass burning emissions: photochemical synthesis, calibration, chemical characterization, and first atmospheric observations†

James M. Roberts, *[a] J. Andrew Neuman,[ab] Steven S. Brown,[a] Patrick R. Veres,[a] Matthew M. Coggon,[a] Chelsea E. Stockwell,[ab] Carsten Warneke,[a] Jeff Peischl[ab] and Michael A. Robinson[ab]

The recent increase in frequency and severity of wildfires in the western U.S. has renewed interest in understanding the impact of wildfire emissions on the chemistry of the atmosphere. Furans are a major class of compounds which are important in wildfire emissions and whose atmospheric reaction mechanisms and fates are relatively understudied. One member of that family, the acyl peroxynitrate that is produced from furfural, furoyl peroxynitrate (fur-PAN) is of interest as a potential participant in oxidant and secondary organic aerosol formation, and is a marker for VOC–NO_x photochemistry from wildfire. This work describes a simple photochemical method for synthesizing fur-PAN and demonstrates its detection with thermal decomposition iodide ion chemical ionization mass spectrometry. Fur-PAN has been observed at up to 140 pptv in ambient measurements in Pasadena, CA, in the summer of 2021 during a brief period of wildfire impact at that site, and fur-PAN was well correlated with acryloyl peroxynitrate (APAN), another wildfire photochemical product. Laboratory measurements of fur-PAN thermal decomposition showed it to be similar to other PAN-type compounds and can be described by the Arrhenius expression: $k = 3.7 \pm 0.2 \times 10^{16} \exp(-(13\,700 \pm 500)/T)\ s^{-1}$. The solubility of fur-PAN in pure water was also measured and found to be 12.9 ± 0.9 M atm^{-1} at 295 K, approximately 3–12 times more soluble than other simple alkyl PAN compounds. Thermal decomposition will be a major loss process for fur-PAN in the daytime boundary layer, but there may be a contribution from hydroxyl radical reactions.

Received 8th June 2022
Accepted 15th July 2022

DOI: 10.1039/d2ea00068g

rsc.li/esatmospheres

Environmental significance

Wildfires (WF) are a persistent air quality problem in North America. Better understanding of the chemistry of WF emissions is essential to the prediction and management of the impacts of these sources on populations and ecosystems. The compound studied here, furoyl peroxynitrate, is a key product that can serve as a useful tracer of the oxidant and secondary particle formation chemistry occurring in WF plumes.

1 Introduction

Air pollution from wildfire has become one of the more challenging air quality issues in the U.S. and has been growing in importance due to larger and more frequent wildfire in the U.S.[1] The air quality management of wildfires requires detailed understanding of the emissions and processing of volatile organic compounds (VOCs) and oxides of nitrogen ($NO_x = NO + NO_2$) associated with this source. Improvements in the quantitative description of this VOC–NO_x photochemistry will aid in predicting the severity and geographic extent of wildfire air quality impacts on O_3 and secondary organic aerosol (SOA) production.

The photochemistry of VOCs in the presence of NO_x is central to the production of oxidants, including O_3, and the chemistry that leads to SOA formation. Furans are one of the classes of VOCs that have been identified as being especially important in wildfire emissions and are understudied in terms of product formation and ultimate fate.[2–6] The furans as a family

[a]NOAA Chemical Sciences Laboratory, Boulder, CO, 80305, USA. E-mail: James.M.Roberts@noaa.gov

[b]Cooperative Institute for Research in Environmental Sciences, NOAA, University of Colorado Boulder, Boulder, CO, 80309, USA

† Electronic supplementary information (ESI) available. See https://doi.org/10.1039/d2ea00068g

are emitted by wildfire from the pyrolysis of cellulose and hemicellulose[7] and the first few mechanistic steps in their photochemical processing has been described from laboratory studies and more recently implemented into atmospheric models of wildfire smoke.[4,8,9] The primary members of this family are furans, alkyl furans, and furfural (C_5H_4O), the C_1 aldehyde of furan. The photochemical processing of furan involves both stepwise oxidation of the 2- and 5-position carbons to form furanone and then maleic anhydride and ring-opening mechanisms that form di-functional C_4 compounds that are formic acid esters. The oxidation of furfural by OH proceeds either by addition to the ring or abstraction of the aldehyde hydrogen, with H abstraction thought to be the major reaction pathway.[10] The resulting acyl radical [$RC(O)^{\bullet}$] can react with O_2 and then NO_2 to form an acyl peroxynitrate, [$RC(O)OONO_2$], a set of reactions common to the formation of all acyl peroxynitrates.

$$RC(O)OO + NO_2 + M \rightarrow RC(O)OONO_2 + M \quad (R1)$$

$$RC(O)OONO_2 + M \rightarrow RC(O)OO + NO_2 + M \quad (R2)$$

$$RC(O)OO + NO \rightarrow R + CO_2 + NO_2 \quad (R3)$$

Acyl peroxynitrates have been given the acronym "PAN-type compounds" and are common products of VOC–NO_x photochemistry.[11–13] The PAN-type compound resulting from furfural is termed furoyl peroxynitrate, using the radical-peroxynitrate naming convention [$RC(O)–OONO_2$], and will be referred to by the acronym fur-PAN in this paper. Furfural also reacts with nitrate radical (NO_3), ($k = 9.07 \times 10^{-14}$ cm^3 per molecule per s), but H abstraction from the aldehyde is probably only a minor pathway of that reaction.[14]

The chemistry of PAN-type compounds has been the subject of considerable research because their presence and relative abundance is governed by the VOC–NO_x photochemistry occurring in a given airmass and PAN-type compounds can be reservoir species that effectively transport NO_x over long distances. The most abundant PAN-type compound is acetyl peroxynitrate ($CH_3C(O)OONO_2$) which has a long history in air pollution chemistry[11] and atmospheric chemistry in general.[15] Many VOC species oxidize eventually to acetaldehyde or other compounds that yield acetyl radical such as methyl glyoxal, making acetyl peroxynitrate the most abundant PAN-type compound.[12] It should be noted that the simple C_1 compound, formyl peroxynitrate, does not form in the atmosphere because the reaction of formyl radical with O_2 yields hydroperoxyl radical (HO_2) and carbon monoxide (CO). Other PAN-type compounds are generally less abundant than PAN, but have been shown to be good indicators of the VOCs that are contributing to the photochemistry in particular locations.[16–18] Although numerous other PAN-type compounds are known[19] only a handful of them have been observed in the atmosphere: propionyl (PPN), acryloyl (APAN), methacryloyl (MPAN), i-butyryl (PiBN), *n*-butyryl (PnBN), and benzoyl (PBzN) peroxynitrates. Fur-PAN is a newly observed compound that to our knowledge has not been reported in atmospheric measurements before. As it is produced from furfural, fur-PAN is expected from biomass burning (BB) VOCs that have undergone ambient photochemistry.

The loss of PAN-type compounds from the atmosphere governs the range and degree of their impact on NO_x transport and the scope of their influence on oxidant and SOA chemistry. Only two processes are important for loss of PAN, thermal decomposition and photolysis, since reactions with atmospheric radicals (OH, Cl) are too slow to be important and PAN is not very soluble in aqueous solution.[19] PAN-type compounds are thermally unstable at temperatures characteristic of the summertime mid-latitude planetary boundary layer, with the known examples all having decomposition rates that vary over an order of magnitude at a given temperature, depending on the compound.[20,21] The differences in thermal decomposition rates amongst PAN-type compounds is sometimes reflected in changes in their relative abundance under surface transport conditions.[22] Therefore, the thermal decomposition rate is an important parameter for predicting the atmospheric behaviour of a given PAN-type compound. The thermal decomposition rates of PAN-type compounds at lower temperatures characteristic of the mid-to upper-troposphere are quite slow, leading to thermal lifetimes of months. Under these cold conditions, other loss processes such as photolysis,[23,24] radical reactions with OH or Cl atoms, or heterogeneous uptake can become important, depending on the nature of the particular acyl group. For example, MPAN has a relatively large rate constant towards reaction with OH radicals due to its unsaturated backbone (2.9×10^{-11} cm^3 per molecule per s),[25] and it is therefore expected that APAN would have a significant rate constant against reaction with OH ($\sim 1.5 \times 10^{-11}$ cm^3 per molecule per s).[26]

The heterogeneous uptake of atmospheric trace gases is usually governed by their aqueous solubility since most surfaces are of that nature. The aqueous solubilities of PAN-type compounds studied to date are generally quite low (2–4 M atm^{-1}), and their hydrolysis rate constants are relatively slow ($2.4–7.4 \times 10^{-4}$ s^{-1}),[27–29] despite the presence of the peroxynitrate group. Solubility in *n*-octanol has only been measured for PAN,[30] and is 8–10 times higher than for pure water, however the limited environmental surface area for this type of material (*e.g.* organic aerosol) yields only a very small effective loss by this process. All of the above studies have been limited to alkyl-PAN compounds. The presence of the hetero-atom ring in fur-PAN prompts an interest in measuring solubilities and solution reaction rates to assess their importance to fur-PAN loss processes.

Several synthetic routes have been developed for PAN-type compounds in addition to the main atmospheric pathways. Liquid phase syntheses have centred around reaction of the corresponding peroxycarboxylic acid with a strong nitrating agent.[11,31,32] This method works well for compounds resistant to side reactions that can occur in the presence of strong reagents (*e.g.* hydrogen peroxide, concentrated sulfuric acid). Several selective photochemical methods have been developed that use either ketones, diketones, or acid chlorides to yield the desired acyl radical.[33–35] These photochemical sources rely on rapid formation of an excess of the desired RC(O)OO radical to

convert a calibrated amount of an NO standard to NO_2 through reaction (R3) and subsequent reactions of hydroperoxyl radicals with NO. The desired PAN compound is then formed through (R1). Conditions can be devised such that a stable, highly efficient (≥93%) conversion of the NO standard can be achieved and used as a stable calibrant.[33,35,36] The reaction of bromine atom (Br) with aldehydes in the presence of NO_x has been used as relatively efficient method for making PAN compounds because of the selectivity of abstraction reactions with aldehyde hydrogens.[21,37]

This paper presents a method for the photochemical synthesis of fur-PAN using the photolysis of Br_2 in the presence of furfural and nitric oxide (NO) in air. We also describe the room temperature gas chromatographic (GC) separation of fur-PAN that can be used to calibrate the fur-PAN output by thermal conversion with a total odd-nitrogen (NO_y) catalyst and detection as NO. The response of a thermal decomposition iodide ion time-of-flight chemical ionization mass spectrometer (TD-I^- ToF-CIMS) to fur-PAN was measured and compared to those of other PAN-type compounds. Preliminary measurements of fur-PAN in an urban area impacted by wildfire are briefly described. The photochemical source was used for the determination of fur-PAN thermal decomposition kinetics, and the aqueous solubility of fur-PAN. The implications of these chemical processes for the atmospheric chemistry of fur-PAN are assessed.

2 Experimental approach

2.1. Fur-PAN photochemical source

The fur-PAN photochemical source used in this work was based on Br_2 photolysis and the selective reaction of Br atoms with aldehydes, in this case furfural. The source, shown schematically in Fig. 1, is relatively simple and compact, and the Br_2 absorption cross section and LED emission spectrum are shown in Fig. S1.† The light source consists of a Luxeon Quad LED module (SZ-05-S8) rated at 2.7 W, with a central wavelength of 405 nm and 12 nm FWHM, powered by a LuxDrive A011-D-V-500 current driver. The photolysis cell is constructed of borosilicate (Pyrex) glass in the dimensions shown. The Br_2 is supplied by a permeation device containing liquid Br_2 (VICI Metronics), has a nominal output of 600 ng min^{-1} at 40 °C and was swept into the photocell with a flow rate of 10 sccm of air. The furfural source consists of a diffusion cell system (1 mm ID, 5 cm length capillary), described previously[38,39] filled with liquid furfural (99% Sigma-Aldrich), and temperature controlled at 70 °C. The flowrate through the diffusion cell system was 28 sccm in initial studies, calibration, and solubility studies, and later increased for the thermal decomposition studies that required a range of residence times. Nitric oxide is supplied to the source by adding 10 sccm of a 1.78 ppmv NO standard in N_2. The mixing ratios of these reactants in the photocell were approximately 1.75 ppmv of Br_2, 370 ppbv of NO, and 4.9 ppmv of furfural and the photocell pressure was room pressure (nominally 625 torr).

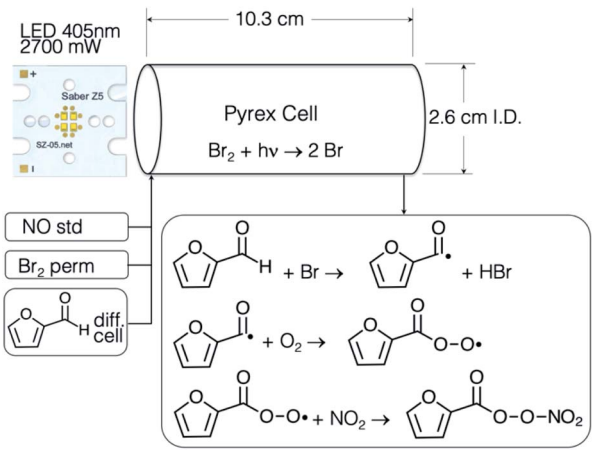

Fig. 1 Schematic of the fur-PAN photochemical source and associated chemistry.

2.2. GC separation

The GC system used for the separation of the photocell effluent is the same system that was described previously.[34] It consists of a 6-port valve, a short GC column under a carrier gas flow of 10 sccm helium, with the effluent directed either into an NO_y instrument or an I^- CIMS instrument. The sample was introduced to the column by discrete injection with a 2 cm^3 sample loop. A number of different GC columns were tested: Rtx-200 (trifluoropropyl silicone), 15 m and 2 m lengths, 0.53 mm ID, 1.5 μm film thickness; Rtx-1701 (cyanopropyl silicone), 1.5 m, 0.53 mm ID, 1 μm film thickness; 5 m of PFA tubing, 0.51 mm ID; and Rtx-1 (methyl silicone), 2 m, 0.53 mm ID, 1.5 μm film thickness. All of the columns were operated under a flow of 10 sccm of helium. In the final configuration, the 2 m Rtx-1 column was connected to the high flow NO_y or I^- CIMS inlets directly through a PFA tee, minimizing PFA surfaces downstream of the GC column. The columns were kept at room temperature (21 ± 2 °C) in order to minimize thermal decomposition. The GC was used for calibrations as well as the thermal decomposition experiments described below, and the room temperature varied less than 2 °C over the short time scales of those experiments.

2.3. NO_y calibration system

The NO_y system used for calibration of the fur-PAN eluting from the GC column is the same as used previously,[34] and is based on the conversion of PAN-type compounds to NO on a molybdenum oxide (MoO_x) catalyst, with detection of the resulting NO by NO–O_3 chemiluminescence. The MoO_x catalyst was operated at 450 °C in air with addition of a small flow of H_2 (~5 sccm) to ensure the MoO_x stayed in a consistent oxidation state. The catalyst conversion efficiency was routinely checked by O_3-titration of the NO standard to NO_2 and measurement of the NO_2 reconversion through the catalyst. The GC effluent was added to the NO_y system directly in front of the NO_y catalyst, and the GC peaks were integrated after subtraction of any baseline signal. Uncertainties in the measurements of the fur-PAN standard are estimated from the combined uncertainties of flow rates (±2%), NO standard concentration (±1%), NO_y

conversion efficiency (95 ± 5%), and the reproducibility of the GC runs (relative standard deviation < 5%).

2.4. I^- CIMS instruments

Two different chemical ionization mass spectrometer (CIMS) systems that employed iodide ion ionization were used in this study: the time-of-flight CIMS (I^- ToF-CIMS) described by Veres *et al.*,[40] and the I^- quadrupole CIMS system described previously.[41–43] The I^- CIMS method for PAN-type compound detection relies on the thermal decomposition (*via* (R2)) immediately in front of an aperture leading to the ion molecule reaction (IMR) region in which the following reaction takes place:

$$RC(O)OO + I^-(H_2O) \rightarrow RC(O)O^- + IO + H_2O \quad (R4)$$

with the carboxylate ion being detected by the mass spectrometer. The I^- ToF-CIMS employed a pressure-controlled inlet and a pressure- and water vapor-controlled IMR. Notably, the I^- ToF-CIMS operates at lower IMR pressure (40 mbar rather than 100 mbar used in other instruments), in order to minimize the impact of possible secondary chemistry in the IMR. The flow conditions and pressure in the IMR correspond to an approximate residence time of 45 ms. The thermal dissociation inlet consisted of 30 cm of 6.4 mm ID PFA tubing, temperature controlled at 130 °C. I^- ions were produced by vacuum UV photolysis of CH_3I using a krypton discharge lamp.[44]

The quadrupole instrument was based on the one described by Slusher *et al.*[43] for the measurement of PAN-type compounds. It had a heated inlet consisting of a 9.5 mm OD 7.5 mm ID PFA tube that could be temperature controlled between room temperature and 200 °C. Iodide ions were produced in a ^{210}Po ionizer (NRD) through which CH_3I in N_2 was flowed. The IMR was held at 20 or 22 torr pressure and had a residence time of approximately 60 ms. The ions were sampled through a collisional-dissociation chamber (CDC) and then passed into a lower pressure chamber (0.2 torr) containing octupole ion guides. The inlet system of the quadrupole CIMS was also fitted with a loop of stainless steel tubing that was heated to 200 °C and could be switched in-line to thermally decompose PAN-type compounds prior to analysis by the PAN CIMS, effectively providing an instrument zero signal and a qualitative diagnostic for PAN-type compounds.

2.5. Field measurements

Field measurements of fur-PAN and other biomass burning tracers were conducted during the 2021 Southwest NO_x and VOC Experiment (SUNVEx, https://csl.noaa.gov/projects/sunvex/). SUNVEx was a two-part ground campaign conducted to study air quality in Las Vegas and Los Angeles (LA) Basin during the summer ozone season.

Ground measurements were conducted from Aug 2–September 5, 2021 at the California Institute of Technology in Pasadena, CA (Fig. S6†). The ground site hosted a suite of gas-phase instrumentation, including the I^- ToF-CIMS described previously. All instruments sampled air from a 10 m tower located within 1 km of the measurements conducted during the 2010 CALNEX campaign.[45] Meteorological data were measured at the top of a nearby building with a TCCON ZENO Weather Station (Coastal Environmental Systems).

VOCs were measured using a proton-transfer-reaction time-of-flight mass spectrometer (PTR-ToF-MS).[46] The PTR-ToF-MS sampled air through a 10 m Teflon inlet at 2 L min^{-1}. Mass spectra were reported every minute, and instrument backgrounds were determined every 2 h by passing ambient air through a platinum catalyst heated to 350 °C. VOC mixing ratios were determined using a custom-built liquid calibration system. Here, we report the mixing ratios of furfural.

Carbon monoxide was measured by off-axis integrated cavity output spectroscopy (F-N_2O/CO-23r, ABB Inc./Los Gatos Research[47]). Ambient air was sampled approximately 10 m above ground level through a *ca.* 10 m stainless steel tube (3.2 mm OD, 1.6 mm ID) and data were recorded at 1 Hz. Final data were reported as 1 minute averages. The instrument was calibrated in the laboratory to the World Meteorological Organization CO_X2014A scale[48] immediately before and after the field project. The precision of the 1 minute data was 0.2 ppbv, and the estimated uncertainty is 1%. All data are reported as dry air mole fractions.

On August 14, 2021, a small fire ignited at a local park within 8 km SW of Pasadena. Smoke was transported to the ground site and sampled by a suite of gas-phase instrumentation. We report measurements from this period to illustrate the presence and atmospheric abundance of fur-PAN from a young biomass burning plume.

2.6. Thermal decomposition method

The thermal decomposition rate of fur-PAN was quantified by measuring the decrease in fur-PAN signal after passing through a reaction volume for a given time at a fixed temperature. The experimental set-up (schematic diagram shown in Fig. S2†) consisted of a PFA reaction volume (250 cm^3 or 1000 cm^3 nominal volumes), to which the fur-PAN source was added along with a 7.5 sccm of 100 ppmv NO in N_2 mixture. The volumes of the reactors were measured by weighing them before and after filling them with water. The relatively high concentration of NO (5–15 ppmv) prevented the reformation of fur-PAN by reaction (3) so that the reaction rate being measured was that of reaction (2). The presence of high NO would interfere with the I^- CIMS measurements which rely on the detection of the RC(O)OO radical (see Zheng *et al.*, 2011 (ref. 42) for an example), so the mixture that exited the reactor was separated by the GC system prior to detection by I^- CIMS. The reaction times at each temperature were corrected for temperature and pressure (625 ± 5 torr) and were varied somewhat by changing the flow rate of zero air through the furfural diffusion source. The change in absolute concentration of fur-PAN that resulted from this flowrate change did not impact the experiment because only the change in relative concentration before and after the reactor was germane to the experiment (provided the response of the I^- CIMS is linear in the applicable range):

$$C_t/C_0 = \exp(-k_d t_r) \quad (1)$$

where C_0 and C_t are the concentrations of fur-PAN before and after reaction, which were determined by GC analysis of 3 to 5 samples taken directly from the fur-PAN source compared to samples taken with the reaction vessel in-line. The ratio C_t/C_0, along with reaction time t_r, allowed the calculation of k_d, the first order loss rate constant corresponding to reaction (2). Thermal decomposition rates of PAN-type compounds are known to obey the simple Arrhenius expression (see Kirchner *et al.*, 1999 (ref. 20) and references therein):

$$k_d = A \exp(-E_a/RT) \quad (2)$$

The preexponential factor, A, and activation energy, E_a were obtained by measuring k_d at a number of temperatures, between room temperature and 50 °C and will be compared to the extensive results for other PAN-type compounds in the Results section below. The uncertainties in the measurements were derived from uncertainties in the flow rates corrected for temperature and pressure, which were 5% or less and the variability of fur-PAN measurements made under the same conditions, *i.e.*, replicate samples, which varied from less than 2% relative standard deviation (RSD) to slightly above 20% RSD.

2.7. Henry's law solubility measurement

Henry's law solubilities of fur-PAN under a variety of conditions and in several media were measured using bubble flow reactors in the same manner as described by Kames *et al.*, (1991),[28] Kames and Schurath,[27] Roberts,[30] and Roberts and Liu.[49] Fig. S3† shows a schematic diagram of the experimental set-up. The flow system consisted of a humidifier and reactor in series with a 3-way valve connected between them that allowed fur-PAN to be introduced and removed from the reactor without opening the system and perturbing the main flow. The humidifier and reactor were placed in a water bath that permitted the temperature to be controlled within ±0.5 °C. Liquid sample volumes in the range 10–25 mL were used in the experiments. The main flow of zero air was controlled by a 1000 sccm mass flow controller and measured at the reactor exit periodically to account for the addition of water vapor to the flow system. Flows were varied from 125 to 1280 cm^3 min^{-1} at ambient temperature and pressure. The effluent of the flow reactor was connected to the inlet of the I^- CIMS by means of a tee, and the remainder of the instrument flow (~2.2 SLPM) was supplied by either room air or humidified zero air. A series of equilibration experiments were conducted by introducing the small flow of the fur-PAN source through the 3-way valve to the reactor containing a known volume of liquid and monitoring the amount of fur-PAN exiting the reactor. When this signal plateaued, the fur-PAN source was switched out of line and the decay of the fur-PAN signal monitored. The flow reactors were constructed to provide a large volume of finely-divided bubbles, maximizing mass transfer between the gas and liquid phases. Under conditions in which the gas–liquid equilibrium within the bubble flow reactor is rapid relative to the residence time within the reactor, this decay signal is an exponential that obeys the following relationship:

$$\ln(C_0/C_t) = [\phi/(HRTV) + k_h]t \quad (3)$$

where C_0 and C_t are the concentrations of the analyte exiting the reactor at time = 0 (the time the fur-PAN source was turned off) and at time, t, after the source was turned off. V is the liquid volume (mL), ϕ is the flow rate in ambient cm^3 s^{-1}, H is the Henry's coefficient (M atm^{-1}), k_h is the first order loss rate constant in solution (s^{-1}), and RT is the ideal gas constant and temperature (R = 0.08206 L atm deg^{-1} mol^{-1}, T is in K). According to eqn (3), the decay rates observed for a series of experiments at different ϕ/V should have a linear relationship with the slope = $1/HRT$ and an x-intercept = k_h. In practice, the rapid equilibration conditions of the bubble reactor are demonstrated by consistency of experiments performed at a range of ϕ and V, but yielding the same ϕ/V.

3 Results and discussion

3.1. Br_2 photolysis and fur-PAN production

The photosource chemistry relies on efficient photolysis of Br_2 to produce Br atoms. The photolysis rate of Br_2 due to the 405 nm LED was measured by monitoring the decrease in the I^- CIMS signal at $I{\cdot}Br_2^-$ when the LED was turned on (see Fig. S4†), and was found to be 5×10^{-2} s^{-1}, and corresponded to 93% Br_2 photolysis at the flow conditions used for most of this study. While Br atoms can react with other species in the system, for example by Br atom recombination, reaction with NO, NO_2 or RO_2 radicals, the reaction of Br atoms with furfural is thought to be exclusively by abstraction of the aldehyde hydrogen, leading to the desired acyl and peroxy acyl radicals. The initial reactions of the peroxyacyl radicals will convert NO to NO_2 and will result in a number of organic radicals from the decomposition of the furoyl carboxyl radical RC(O)O. Thus, there are a number of pathways to smaller (*i.e.* $\leq C_4$) compounds. Once sufficient NO is converted to NO_2, the furoyl peroxy radical will react with it to form fur-PAN. Mass spectra of the output of the fur-PAN photosource added to ambient air through the hot PAN inlet (150 °C) and through the inlet at room temperature PFA are shown in Fig. 2. There are several features apparent in the comparison of the hot and cold inlet signals; the major peak in the hot inlet is m/z 111 corresponding

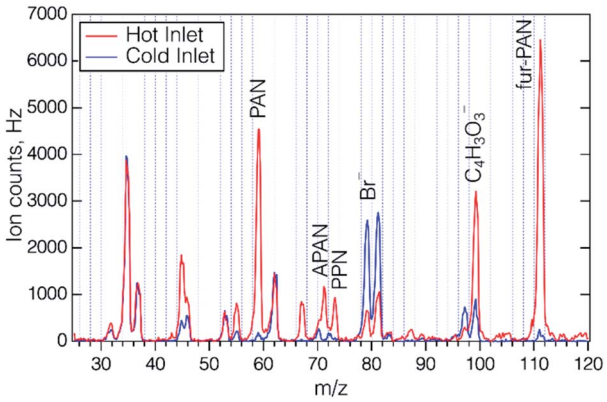

Fig. 2 Mass spectra of the output of the fur-PAN source added to ambient air and measured with the quadrupole I^- CIMS, through the heated (red) and cold (blue) PAN inlet.

to furoate, the carboxylate ion resulting from reaction of the furoyl peroxy radical with I^-, and a peak at *m/z* 99 that was nearly half the size of that of furoate. The high resolution I^- ToF CIMS found that the *m/z* 111 peak had the proper exact mass, 111.008, corresponding to furoate ($C_5H_3O_3^-$), and that the ion at *m/z* = 99.008 corresponded to an empirical formula of $C_4H_3O_3^-$, which we assign to the 4-oxo-2-butenoate ion [HC(O)CH=CHC(O)O$^-$]. The fact that *m/z* 99 is higher through the hot inlet implies that the corresponding C_4 PAN-type compound [termed OB-PAN here] might be formed in the photosource. Also evident were the carboxylate ions corresponding to the common PAN-type compounds: PAN (*m/z* 59), acryloyl peroxynitrate (APAN, *m/z* 71), and propionyl peroxynitrate (PPN, *m/z* 73), that were present in room air without any added chemical source. The only ions that appear larger in the cold inlet were Br^- and $Br\cdot H_2O^-$. While these ions are most assuredly due to the Br_2 in the photosource, it is not immediately clear why those ions particular were more abundant in the cold inlet.

3.2. Dependence of I^- CIMS response on inlet temperature

The dependence of the carboxylate signals from PAN-type compounds on inlet temperature can be a useful diagnostic and helps to determine the optimal set-up for ambient measurements.[34,42,50,51] The optimum temperature for decomposition will depend on the geometry and residence time of the inlet, and the nature of the PAN-type compound. The R(CO)OO–NO_2 bonds in these molecules, where R is a hydrocarbon, all have very similar bond strengths (±4 kJ mol^{-1}) as discussed below, but the fate of the RC(O)OO radical can vary widely depending on R. The extreme case is the methacrylyl peroxy radical, [CH_2=C(CH_3)C(O)OO], which seems to thermally decompose quite readily, as indicated by the much lower response of the PAN-CIMS to MPAN.[34,42,43,51] Conversely, the saturated alkyl peroxyacyl radicals such as $CH_3C(O)OO$ and $CH_3CH_2C(O)OO$, appear to be quite stable up to the limits of inlet temperatures that have been explored (~200 °C).[34,42,50,51] The profiles of furoate and 4-oxo-2-butenoate ions from the fur-PAN source are plotted in Fig. 3 as a function of PAN inlet temperature, shown as a fraction of the response normalized to the highest response. Also shown is the ratio of 4-oxo-butenoate to furoate, which increased steadily with temperature. The PAN-inlet has only a modest effect on the IMR temperature (12 °C at a PAN-inlet temperature of 200 °C), which has a negligible effect on the rate of (R4).[52] The furoate temperature profile maximizes at approximately 150 °C and indicates that the peroxyfuroyl radical undergoes some thermal decomposition. The thermal decomposition profiles of acetyl peroxynitrate and the appearance of *m/z* 99 are virtually identical in this PAN inlet. Previous studies have shown that these temperature profiles differ somewhat between instruments depending on specific inlet residence times and geometries.[34,42,50,51]

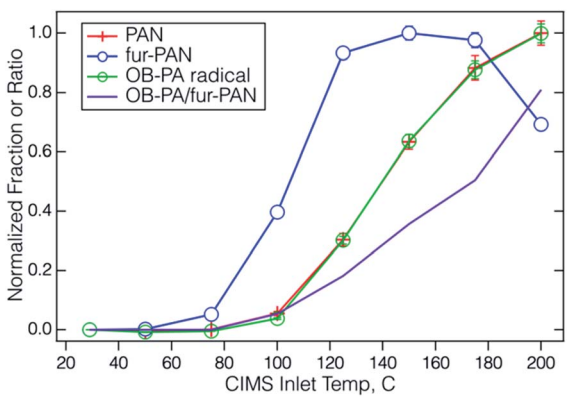

Fig. 3 The temperature profiles of the I^- CIMS response to PAN and fur-PAN plotted relative to their highest signal, along with the signal at *m/z* 99 tentatively assigned to OB-PAN.

3.3. GC separation of compounds coming out of the fur-PAN source

The amount of a given PAN-type compound coming out of the photosource can be determined by conversion to NO or NO_2 and detection by NO–O_3 chemiluminescence or cavity ring-down optical absorption, respectively.[33,34,51] However, the complicated chemistry exhibited by the photosource used in this work necessitates the use of GC separation prior to analysis to ensure the desired PAN-type compound is isolated. The separation of the output of the fur-PAN source was especially needed given the presence of 4-oxo-2-butenoate in the mass spectrum of the source.

As described in the Experimental approach section, a number of GC columns were tried for separation of fur-PAN and OB-PAN prior to measurement by I^- CIMS or NO_y systems. The column originally used by Veres and Roberts (2015)[34] for the separation of C_2–C_4 PAN-type compounds: Rtx-200 (trifluoropropyl silicone), 15 m length, 0.53 mm ID, and 1.5 μm film thickness did not result in an observable peak for either fur-PAN or the suspected OB-PAN compound, on either I^- mass spectrometer system. A 2 m length of the same column material did elute both species, but both had retention times of 11.5 min. Subsequent attempts to separate the two species with the Rtx-1701 and PFA tube columns were unsuccessful, with both columns eluting the two compounds at the same time, and in some cases (PFA) with considerable (identical) peak tailing. This chromatographic work indicated that fur-PAN is more polar than the typical C_2–C_4 PAN-type compounds. As a consequence, a short length of the non-polar Rtx-1 column was employed and the column added to the high flow inlets of the CIMS or NO_y instruments directly, *i.e.* with no PFA low-flow transfer lines. An example chromatogram from the short Rtx-1 column is shown in Fig. 4, which shows the coincidence of the furoate and 4-oxo-2-butenoate signals. This coincidence of the furoate signals, from fur-PAN, and the OB anion in both retention time and peak shape in all the chromatographic systems implies that the OB anion may not be from a separate product of the photosource but rather results from a peroxy radical produced in the PAN inlet.

3.4. Thermal decomposition of the peroxyfuroyl radical

The possibilities that the signal at *m/z* 99 is either from OB-PAN produced in the photosource, or from 4-oxo-2-butenoyl peroxy

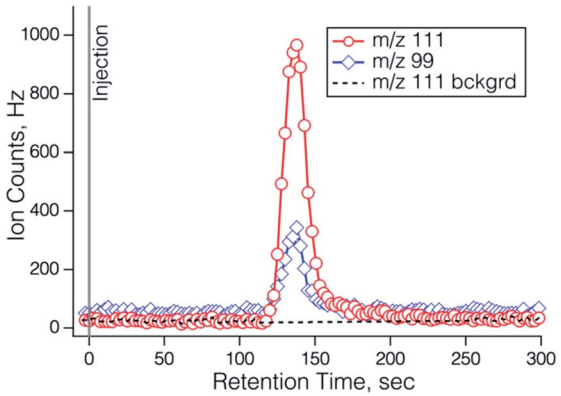

Fig. 4 GC trace during the separation of the effluent of the fur-PAN source on a 2 m Rtx-1 column, 0.53 mm ID, 1.5 μm film thickness. The furoate anion (*m*/*z* 111) is shown in red and the 4-oxo-2-butenoate anion (*m*/*z* 99) is shown in blue.

radical (OB-PA) formed from radical decomposition in the PAN inlet were examined by changing the residence time and concentrations of reactants in the photosource with the expectation that the relative amounts of OB-PAN and fur-PAN would be different, since OB-PAN would require a longer reaction time to form. However, the relative amounts of *m*/*z* 99 and *m*/*z* 111 were the same regardless of the change in photosource conditions, as shown in Fig. S5.† Moreover, this constant ratio is the same in the GC separation experiments. This, coupled with the thermal decomposition data shown in Fig. 3 is persuasive evidence that *m*/*z* 99 arises from decomposition of peroxyfuroyl radical in the PAN inlet. Furan-type compounds are known to undergo relatively facile ring-opening reactions when the carbons on either side of the ring O atom are oxidized.[5,8,10,53] Accordingly, two possibilities exist for the decomposition of the furoyl compound, as shown in Fig. 5: (I) the peroxyfuroyl radical could undergo a cyclic rearrangement involving a 6-member ring, eliminating CO_2 and forming the oxo-butenoyl radical which would rapidly react with O_2 to form the OB-PA radical: (II) the peroxyfuroyl radical could form the corresponding acyloxy radical [RC(O)O], through either self-reaction or reaction with NO, followed by cyclic rearrangement of that acyloxy radical. The efficiency of pathway II would be very dependent on absolute concentrations of RO_2 radicals and/or small amounts of NO, in addition, acyloxy radicals are known to rapidly decompose to CO_2 and an organic radical, R. Therefore, pathway I is by far the most likely given the invariance of the ratio of OB to furoate under changing conditions in the photosource and PAN inlet.

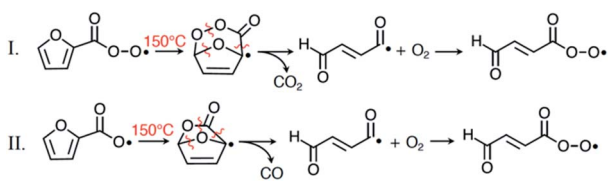

Fig. 5 Possible radical decomposition pathways occurring in the PAN inlet.

The cyclic rearrangement of the peroxyfuroyl (fur-PA) radical is analogous to other internal rearrangements that have been associated with auto-oxidation mechanism of organic species having 4 or more carbons.[54] The 1 and 4 carbons of the furan ring are particularly favourable sites for this chemistry due to the facility with which conjugated systems can form, involving the conversion of the ring oxygen to a carbonyl. The temperature profiles in Fig. 3 imply a significant temperature dependence to rearrangement I. However, the extent to which this chemistry can happen at atmospheric temperatures is uncertain at this point because the conditions in the fur-PAN photosource resulted in a much shorter fur-PA radical lifetime than would be present in the real atmosphere. It might be important to revisit the room temperature chemistry since difunctional oxygenates of this kind are important precursors of secondary organic aerosol.

3.5. NO_y calibration

The GC separates fur-PAN from other possible N-containing by-products of the photosource and provides a convenient means to calibrate the I^- CIMS systems. The I^- ToF-CIMS was used for ambient sampling during the Southwest Urban NO_x and VOC Experiment (SUNVEx, NOAA/CSL, 2021 (ref. 55)) project and was calibrated for the common C_2–C_4 PAN-type compounds using the GC conditions described by Veres and Roberts (2015),[34] and for fur-PAN using the optimized conditions specified in this work. Replicate GC runs were performed under the same conditions employing either the I^- ToF-CIMS or the NO_y system as the detector. The NO_y chromatograms had a peak that eluted at the retention time corresponding to the column dead-volume, which was unreacted NO and NO_2 and perhaps low-molecular weight organic nitrates, but no other peaks in the retention time window of fur-PAN. The relative response factors of the PAN-type compounds, given in Table 1, show fur-PAN to be detected at a lower sensitivity compared to PAN, consistent with the thermal decomposition of the fur-PA radical noted above. Recent work by Robinson *et al.*[52] has shown that the response of the I^- CIMS instruments can have a relatively strong dependence on IMR temperature depending on the ionization mechanism, and that the mechanism involved in PAN-type compounds detection as carboxylate ions (R4) does not exhibit a temperature dependence. The fur-PAN sensitivity translates to a detection limit of 1.5 pptv for a 1 s measurement (3σ of the noise) under surface sampling conditions. The overall uncertainty in fur-PAN measurements with this system as deployed was ±20%. These calibrations were applied to the SUNVEx measurements described below.

Table 1 Sensitivities of the I^- ToF-CIMS to PAN-type compounds

Compound	Sensitivity, cts $pptv^{-1}$	Sensitivity relative to PAN
PAN	2.07	1.0
APAN	2.62	1.27
PPN	3.01	1.45
Fur-PAN	0.51	0.25

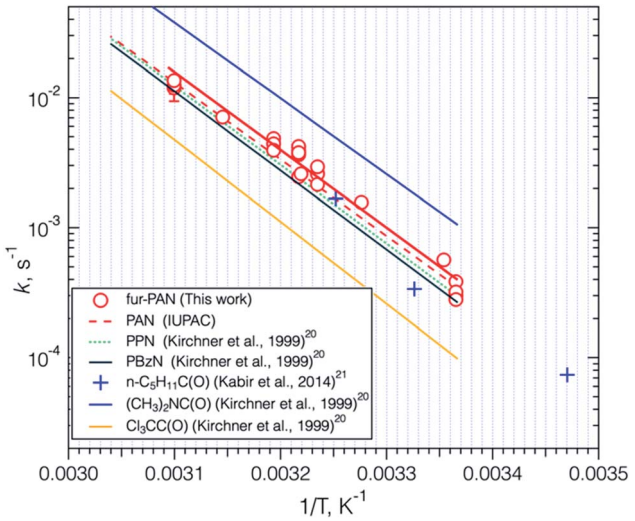

Fig. 6 Arrhenius plot of the thermal decomposition of fur-PAN compared to a number of other acyl peroxynitrate compounds. The individual data points are shown as open circles, with error bars for individual data points, and the fit to the Arrhenius expression is shown as a solid red line. Examples of other Arrhenius expressions are given as noted in the legend, with either the common acronym, or acyl radical, specified.

3.6. Thermal decomposition

Thermal decomposition rate measurements were conducted in PFA reaction volumes as discussed in the Experimental approach section. The resulting first order loss rate constants at each temperature are shown as an Arrhenius plot in Fig. 6. The uncertainties in each rate constant were obtained by propagating the standard deviation of the average of 3–4 measurements before and after reaction, and adding the uncertainty in reaction time discussed previously, in an RMS fashion. These were smaller than the width of the data points in Fig. 6, with the exception of one data point that was ±21%. Also shown in Fig. 6 are the Arrhenius expressions for the common alkyl PANs and the extremes reported by Kirchner *et al.*, (1999),[20] trichloroacetyl peroxynitrate which is particularly stable, and *N*,*N*′-dimethylaminoformyl peroxynitrate which is particularly unstable. The data from IUPAC and Kirchner *et al.* are for 1 bar pressure. The thermal decomposition of PAN-type compounds is known to be pressure dependent,[56] which is well predicted by the expression described by Troe.[57] In general, these rates at 1 bar are close to the high-pressure limit (within 10% of the k_∞). Thus, the thermal decomposition rate constants of fur-PAN measured in this work at 0.833 (±0.007) bar are most likely within 10% of the rate constants at 1 bar and should be suitable for assessing the atmospheric loss in the planetary boundary layer due to this process. The Arrhenius parameters obtained from the fit in Fig. 6 are compared to parameters for other PAN-type compounds in Table 2. Fur-PAN is less stable than most of the common alkyl PAN-type compounds. The only other aromatic compound for which there are literature data, benzoyl peroxynitrate (PBzN), appears to be slightly more stable than fur-PAN, although the uncertainties in the Arrhenius expressions are such that the k values at 298 K are not statistically different from one another. The effect of differences in thermal decomposition rates can sometimes be observed in ambient data in situations where plumes are transported in relatively warm surface layers,[22] so the effect of the faster thermal decomposition rate of fur-PAN might be observable in ambient measurements.

3.7. Solubilities of fur-PAN in aqueous solution

The solubility and hydrolysis rate of fur-PAN in deionized (DI) water were measured at 295 K using the bubble flow reactor method described above. Fur-PAN was detected by the I^- CIMS in the outlet of the reactor added to the main flow of lab air, which had no signal at m/z 111. An example experiment, shown in Fig. S6,† consisted of an equilibration period during which the fur-PAN source was switched into the bubble flow reactor and the fur-PAN signal rose as it equilibrated with the solution, and an exponential decay period after the fur-PAN source was switched out of the system. The data were fit to a simple single exponential equation by linear least squares after conversion to the logarithm. Experiments were performed at several different flow rates, ranging from 120 to 1280 cm^3 min^{-1} (at ambient pressure and temperature) and liquid volumes varying from 10 to 25 cm^3. The decay rate data are plotted *versus* the ratio of the flow rate to liquid volume as shown in Fig. 7. The slope of the data is 1/*HRT* and the *y*-intercept is the first-order rate constant for loss in solution, according to eqn (3), and the uncertainties given are the error estimates from the least-squares fit to the data.

Table 2 Arrhenius parameters for thermal decomposition of fur-PAN and selected PAN-type compounds from the literature

R–$OONO_2$	E_a, kJ mol^{-1}	A, ($\div 10^{16}$), s^{-1}	k^a, s^{-1}	Reference
$CH_3C(O)$[b]	112.9 ± 1.9	2.5	4.1–4.4	20 and 21
$CH_3CH_2C(O)$	115.9 ± 2.2	7.2	3.5	20, IUPAC
n-$C_3H_7C(O)$			3.32 ± 0.13	
$CH_2C(CH_3)C(O)$	112.1 ± 4	1.6	3.5	69
n-$C_4H_9C(O)$			3.42 ± 0.08	21
n-$C_5H_{11}C(O)$			3.38 ± 0.05	21
Fur-PA[c]	113.6 ± 4	3.7 ± 0.2	4.6	This work
$C_6H_5C(O)$	116.4 ± 3.8	7.9	3.1	20

[a] Rate constant at 298 K, 1 bar × 10^4 in s^{-1}. [b] For 0.800 bar. [c] For 0.833 bar.

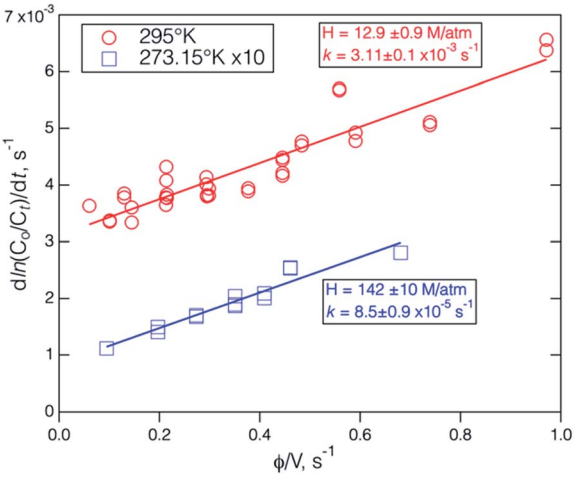

Fig. 7 The results of Henry's law coefficient measurements in DI H_2O at 295 K, and 273.15 K (enlarged ×10 on the *y*-axis). The errors in individual decay rates are smaller than the width of the symbols. The *H* and *k* values and associated uncertainties were obtained from the fit of the data points to eqn (3).

Table 3 Henry's law coefficients for PAN-type compounds in water and in *n*-octanol in comparison with fur-PAN

Compound	Solvent	H, M atm^{-1}	k [×10^4], s^{-1}	Reference
PAN	DI water	3.8–4.1[a]	3.2–6.4	28 and 70
	n-Octanol	42 ± 2.1[b]	0.032 ± 0.25	30
PPN	DI water	2.9 ± 0.06	3.1 ± 0.22	27
PiBN	DI water	1.0 ± 0.03	7.4 ± 0.5	27
MPAN	DI water	1.7 ± 0.16	5.6 ± 1.2	27
PnBN	DI water	2.3 ± 0.06	2.4 ± 0.4	27
Fur-PAN	DI water	12.9 ± 0.9[c]	31 ± 1	This work
		15.8[d]		58 and 59
		140 ± 10[e]	0.85 ± 0.09	This work

[a] 293 K. [b] 291 K. [c] 295 K. [d] Estimated at 298 K. [e] 273 K.

The Henry's coefficient value for fur-PAN at 295 K, measured in this work was 12.9 ± 0.9 M atm^{-1} and the first order loss rate 3.1 ± 0.1 × 10^{-3} s^{-1}, are a factor of 4–10 larger than those measured for the simple alkyl PAN-type compounds, as shown in Table 3. Comparison of the properties of the furan portion of the molecule with those of similar structure like cyclopentane and cyclopentadiene[58] indicate the that likely reasons for the higher solubility of fur-PAN are both the presence of double bonds and the polarity of the ring oxygen. A more quantitative assessment of these effects and the effect of the acyl peroxynitrate group [–C(O)OONO$_2$] can be found in the structure–additivity analysis of Henry's law solubilities presented by Raventos-Duran *et al.*, (2010).[59] Combining the measured Henry's coefficient for furan[58] with the group value for –C(O)OONO$_2$ yields an estimated Henry's coefficient of 15.8 M atm^{-1} at 298 K. Estimated uncertainties of these structure–additivity relationships (SARs) are approximately ±50%, so this estimated H agrees to within expected uncertainties.

The solubility of fur-PAN at ice/water temperature, 140 ± 10 M atm^{-1}, was considerably larger than at room temperature and larger than the Henry's coefficients of PAN and PPN at 273 K, which are approximately 15 and 11 M atm^{-1}, respectively.[27] This follows the expected temperature dependence for organic compounds. The solvation enthalpy ΔH_{soln} and entropy ΔS_{soln} of fur-PAN can be estimated from these data using the Van't Hoff equation and are compared to the values for PAN and PPN in Table 4. The solvation of fur-PAN is about 50% more exothermic than those of the PAN and PPN, possibly because of the polarity of the furan functionality.

Table 4 Solvation enthalpies, ΔH_{soln}, and entropies, ΔS_{soln} for PAN, PPN, and fur-PAN

Compound	ΔH_{soln}, kJ mol^{-1}	ΔS_{soln}, J K^{-1} mol^{-1}	Reference
PAN	−47.4 ± 0.8	−150 ± 2.5	27
PAN	−49.2 ± 4.7	−157 ± 16	71
PAN	−54.2 ± 1.0	−173.1 ± 4	28
PPN	−49.4 ± 0.9	−160 ± 3	27
Fur-PAN	−73.7 ± 7	−230 ± 230	This work

The reaction rate of PAN-type compounds in aqueous solution are about as fast or slightly faster than their thermal decomposition rates at 298 K (Table 2). In contrast, the loss rate of fur-PAN in aqueous solution is about 6 times faster than the thermal decomposition rate at the same temperature. Hydrolysis of PAN is known to be base-catalyzed[60] and the likely mechanism involves formation of the corresponding carboxylic acid and peroxynitrate ($OONO_2^-$), with peroxynitrate being unstable, decomposing to O_2 and nitrite (NO_2^-).[61] The faster rate observed for fur-PAN implies that the rate of this reaction is increased by the polarity of the furan ring.

n-Octanol is a model for organic substrates in the environment, and the ratio of solubilities in *n*-octanol and water can be used to predict where in the environment materials will tend to build up and is also used to predict membrane transport in cellular systems.[62] Unfortunately, attempts to measure the solubility of fur-PAN in *n*-octanol at 295 K were unsuccessful since the signals exiting the bubbler were barely above detection limit. This was true even under conditions in which the fur-PAN/water experiments yielded substantial signals on the I$^-$ CIMS. Previous measurements with acetyl peroxynitrate in *n*-octanol yielded Henry's coefficients higher than for water (Table 3), but slower reaction rates.[30] This implies that our experiments with fur-PAN/*n*-octanol were unsuccessful because of high solubility, not reaction of the –C(O)OONO$_2$ group with the solvent, however this awaits further investigation.

The ultimate lifetime of fur-PAN in the atmosphere will depend on the combination of thermal decomposition, uptake on surfaces due to solubility, and radical reactions, chief among them reaction with OH radical. To our knowledge the reaction of fur-PAN with OH has not been measured. Furan has a relatively fast reaction rate with OH (4 × 10^{-11} cm^3 per molecule per s, see Bierbach *et al.*, (1995)[10] and references therein). However, the –C(O)OONO$_2$ group can decrease reactivity of OH towards the organic group that it is bonded to. For example, k_{ethane} + OH = 2.4 × 10^{-13} cm^3 per molecule per s (ref. 63) and k_{PAN} < 3 × 10^{-14} cm^3 per molecule per s.[23] As a result, we could

expect the reaction of fur-PAN with OH to be slower than for furan + OH. This would result in reaction with OH competitive with thermal decomposition in the daytime boundary layer. The possible reaction of fur-PAN with nitrate radical (NO_3) remains to be investigated.

3.8. Observations of fur-PAN in an urban area

The I^- ToF-CIMS was deployed in Pasadena, CA, during SUNVEx from July 25 to September 15, 2021.[55] The objectives of that experiment were to study the changing photochemical environment of the Los Angeles Basin. Fur-PAN measurements were made along with the other PAN-type compounds and an extensive suite of VOC and other photochemical pollutant measurements. In general, low levels of APAN and fur-PAN (≤10 pptv) were observed throughout the entire measurement period due to limited sources of precursors in the urban area (*e.g.*, acrolein, 1,3-butadiene, and furfural are found in vehicle exhaust). However, California is often impacted by wildfires during the summer months and one such wildfire event was observed during the SUNVEx intensive period, on August 14, 2021. The fire occurred at Ernest E. Debs Park, approximately 8 km southwest of the site (Fig. S7†), and was extinguished within a few hours.[64] The timelines of measurements during this period and resulting correlation plots are shown in Fig. 8a–e. The wildfire emission was observed in two relatively brief plumes, centred around 22:50 and 23:30 UTC (15:50 and 16:30 local daylight time).

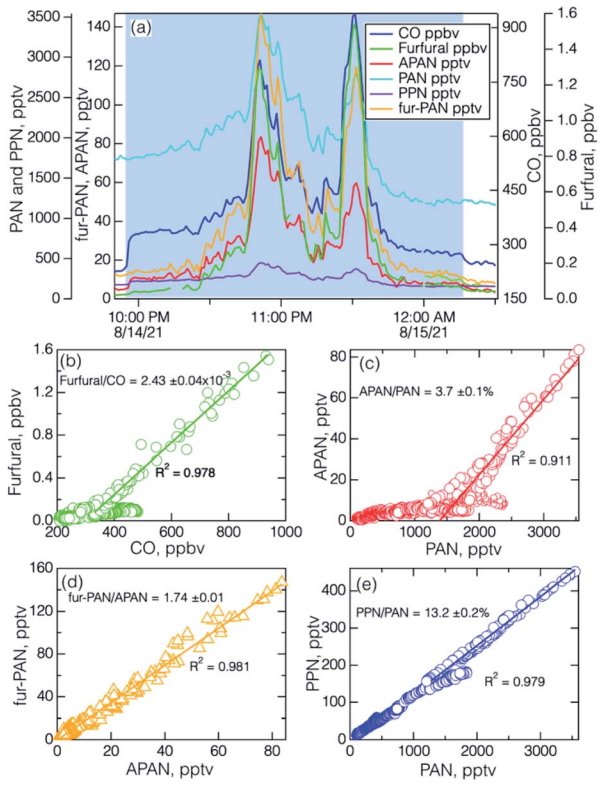

Fig. 8 Observations of a wildfire plume in Pasadena, CA, during the SUNVEx project. Panel (a) shows the timeline (in UTC) of selected wildfire-related compounds, including fur-PAN, with the period during fire impact (21:52 UTC on 08/14/21 to 00:48 UTC on 8/15/21) highlighted in light blue. Panel (b) shows the correlation of furfural and CO for the period 00:00:00 08/14/21 to 23:59:00 08/15/21, and the resulting fit during the wildfire plume. Panels (c–e) show the correlations among the PAN compounds and fits to the data during the wildfire plumes.

Several correlations of primary and secondary wildfire species stand out in the SUNVEx plume. The primary species furfural and CO (Fig. 8b) are quite well correlated ($R^2 = 0.978$), and the slope, 0.243 ± 0.04%, agrees well with the mean value found in the Fire Lab study for the average of all fuel types, 0.24 ± 0.19%.[6] This implies a relatively freshly emitted plume since furfural is much more reactive than CO. The lowest furfural values (*i.e.* ≤0.1 ppbv) correspond to various urban sources, *e.g.* cooking, vehicles, that are much less abundant relative to urban CO. The *x*-intercept: CO ≅ 300 ppbv can be interpreted of as a mean urban value in the absence of a direct source. The wildfire photochemical products, APAN and PAN are also well correlated ($R^2 = 0.911$) in the wildfire plume (Fig. 8c), with a slope of 3.7%, much higher than slopes found in urban areas (≤2%). The lowest APAN values correlate with PAN at a much lower slope, similar to what would be expected in an urban area that has typical vehicular and volatile chemical product sources. Observations of APAN and PAN in BB plumes are relatively scarce, but plumes from agricultural fires in the SE U.S. during the 2013 Southeast Nexus campaign[41,65] had APAN/PAN ratios averaging up to about 5% (see Fig. S8†). The correlation of fur-PAN and APAN during the SUNVEx wildfire plume was quite good ($R^2 = 0.981$) (Fig. 8d), which is to be expected because of the elevated precursor concentrations in wildfire emissions relative to typical urban emissions. To our knowledge, this is the first observation of fur-PAN in the ambient atmosphere, and therefore we have no points of comparison with other data sets. An interesting aspect of these PAN-type compounds is that the starting materials for APAN, acrolein and 1,3-butadiene, are derived from pyrolysis of lignin and cellulosic fuels,[66,67] and the starting material for fur-PAN is derived from pyrolysis of cellulose and hemi-cellulose.[6,7] As a result, we can expect that there will be close correlation of fur-PAN and APAN in a given fire plume, but could vary among different fires because the ratio of the two compounds will depend on the fuel composition and relative abundance of various fuel types. As a matter of interest, the PPN/PAN ratio (13.2%) is in the range that is typically observed in urban areas (10–16%) as is clear from the data from the remainder of the two-day period, and from other urban data sets.[18,19,68,69]

The local wind direction at the SUNVEx site was consistent with transport from the SW, and the wind speed averaged 2.8 ± 0.5 m s^{-1}, corresponding to a transit time of roughly 45 minutes. The SUNVEx wildfire plume is relatively rich in PAN precursors and PAN formation is rapid, a feature that is consistent with previous studies of PAN formation from wildfire and agricultural fires.[70–72] This fire plume is also high in fur-PAN and APAN precursors relative to urban air, so those PAN species are much higher in the wildfire plume relative to urban air. However, the ratio of fur-PAN to furfural is only about 10%, indicating that the air is still relatively fresh (unprocessed). The ratios of PAN-type compounds to precursor aldehydes tend to

reach values up to 1 in urban air masses that have undergone substantial photochemical processing.[73]

4 Conclusions

A photochemical source of fur-PAN was constructed based on the selective reaction of Br atoms with furfural in air containing NO. Bromine atoms were produced by facile (93%) photolysis of Br_2 in a small flow cell illuminated by a 405 nm LED. The initial reaction of Br with furfural occurred primarily through abstraction of the aldehyde-H, resulting in a series of radical reactions. A nitric oxide stream was added to the reactor and was converted to NO_2 and eventually fur-PAN through reactions with peroxy radicals. The output of this photosource was analysed with a quadrupole iodide ion TD-CIMS and the optimum thermal decomposition temperature was found to be 150 °C, slightly lower than that for PAN (200 °C). Direct analysis by TD-CIMS and analysis following GC separation revealed that furoylperoxy radical has a decomposition channel in the TD inlet that leads to a radical with the empirical formula $C_4H_3O_4$, which is believed to be the ring opening product 4-oxo-2-butenyl peroxy radical [HC(O)CH=CHC(O)OO]. GC separation of the photosource effluent allowed calibration by an NO_y instrument and the resulting TD-I^- ToF-CIMS sensitivity was 0.510 Hz $pptv^{-1}$ compared to sensitivity of 2.07 Hz $pptv^{-1}$ for PAN. Observations of fur-PAN during the recent SUNVEx ambient measurements in Pasadena, CA, showed that fur-PAN is generally low (<10 pptv) in this urban area with the exception of a wildfire plume that was sampled briefly on August 14, 2021. During this wildfire plume fur-PAN reached approximately 140 pptv, and there was close correlation of fur-PAN with a number of other wildfire-derived compounds, including APAN, a known wildfire photochemical product. Fur-PAN is unlikely to ever be a large fraction of NO_y in ambient air masses, however it is a marker for the VOC–NO_x photochemistry from cellulose-derived furanoids in wildfire plumes and can have some utility in assessing the nature of fuels that have contributed to, and the extent of photochemical conversion that has happened in, a given plume.

Several experiments were conducted to characterize the chemistry of fur-PAN. The thermal decomposition rate of fur-PAN was found to be slightly higher than those of other common PAN species, with an activation energy, E_a, of 113.6 ± 4 kJ mol^{-1} and pre-exponential factor, A, of $3.7 \pm 0.2 \times 10^{16}$ s^{-1}. The aqueous solubility of fur-PAN was found to be 12.9 ± 0.9 M atm^{-1} at 295 K, approximately 6 times higher than that of PAN, probably due to the polarity of the furan group. This value was in reasonable agreement with a structure–additivity relationship that takes into account the –C(O)OONO$_2$ group. The loss of fur-PAN due to hydrolysis was more than 10 times faster than for alkyl PAN compounds. Attempts to measure the solubility of fur-PAN in *n*-octanol with a bubble flow apparatus were unsuccessful, due to either fast reaction or more likely due to a relatively high solubility. These chemical attributes imply that fur-PAN losses against thermal decomposition or reactive uptake will be faster than for the common alkyl PAN-type compounds. The possible heterogeneous reaction of fur-PAN with organic materials, and the reaction rates with atmospheric radicals and products, remain to be quantified.

Author contributions

JMR designed and built the fur-PAN source. MAR, PRV, JAN, and JMR performed the I^- ToF-CIMS calibration experiments. MAR, PRV, JAN, SSB, MMC, CES, CW, and JP acquired the data during SUNVEx project. JMR performed the thermal decomposition and solubility studies.

Conflicts of interest

There are no conflicts to declare.

Acknowledgements

We thank Paul Wennberg and the California Institute of Technology for hosting the SUNVEx Pasadena experiment and for providing meteorological data. This work was supported in part by the NOAA Cooperative Agreement with CIRES, NA17OAR4320101.

References

1 V. Iglesias, J. K. Balch and W. R. Travis, U.S. fires became larger, more frequent, and more widespread in the 2000s, *Sci. Adv.*, 2022, **8**, eabc0020.
2 J. B. Gilman, B. M. Lerner, W. C. Kuster, P. D. Goldan, C. Warneke, P. R. Veres, J. M. Roberts, J. A. deGouw, I. R. Burling and R. J. Yokelson, Biomass burning emissions and potential air quality impacts of volatile organic compounds and other trace gases from temperate fuels common to the United States, *Atmos. Chem. Phys.*, 2015, **15**, 13915–13938.
3 L. E. Hatch, R. J. Yokelson, C. E. Stockwell, P. R. Veres, I. J. Simpson, D. R. Blake, J. J. Orlando and K. C. Barsanti, Multi-instrument comparison and compilation of non-methane organic gas emissions from biomass burning and implications for smoke-derived secondary organic aerosol precursors, *Atmos. Chem. Phys.*, 2017, **17**, 1471–1489.
4 Z. C. J. Decker, M. A. Robinson, K. C. Barsanti, I. Bourgeois, M. M. Coggon, J. P. DiGangi, G. S. Diskin, F. M. Flocke, A. Franchin, C. D. Fredrickson, G. I. Gkatzelis, S. R. Hall, H. Halliday, C. D. Holmes, L. G. Huey, Y. R. Lee, J. Lindaas, A. M. Middlebrook, D. D. Montzka, R. Moore, J. A. Neuman, J. B. Nowak, B. B. Palm, J. Peischl, F. Piel, P. S. Rickly, A. W. Rollins, T. B. Ryerson, R. H. Schwantes, K. Sekimoto, L. Thornhill, J. A. Thornton, G. S. Tyndall, K. Ullmann, P. Van Rooy, P. R. Veres, C. Warneke, R. A. Washenfelder, A. J. Weinheimer, E. Wiggins, E. Winstead, A. Wisthaler, C. Womack and S. S. Brown, Nighttime and daytime dark oxidation chemistry in wildfire plumes: an observation and model analysis of FIREX-AQ aircraft data, *Atmos. Chem. Phys.*, 2021, 16293–16317, DOI: **10.5194/acp-21-16293-2021**.

5 M. Coggon, C. Y. Lim, A. R. Koss, K. Sekimoto, B. Yuan, J. B. Gilman, D. H. Hagan, V. Selimovic, K. J. Zarzana, S. S. Brown, J. M. Roberts, M. Muller, R. J. Yokelson, A. Wisthaler, K. J. E. Krechmer, J. L. Jimenez, C. D. Cappa, J. Kroll, J. de Gouw and C. Warneke, OH chemistry of non-methane organic gases (NMOGs) emitted from laboratory and ambient biomass burning smoke: evaluating the influence of furans and oxygenated aromatics on ozone and secondary NMOG formation, *Atmos. Chem. Phys.*, 2019, **19**, 14875–14899.

6 A. R. Koss, S. K. Sekimoto, J. B. Gilman, V. Selimovic, M. M. Coggon, K. J. Zarzana, B. Yuan, B. M. Lerner, S. S. Brown, J. L. Jimenez, K. J. Krechmer, J. M. Roberts, C. Warneke, R. J. Yokelson and J. de Gouw, Non-methane organic gas emissions from biomass burning: identification, quantification, and emission factors from PTR-ToF during the FIREX 2016 laboratory experiment, *Atmos. Chem. Phys.*, 2018, **18**, 3299–3319.

7 F. X. Collard and J. Blin, A review on pyrolysis of biomass constituents: mechanisms and composition of the products obtained from the conversion of cellulose, hemicelluloses and lignin, *Renewable Sustainable Energy Rev.*, 2014, **38**, 594–608.

8 S. M. Aschmann, N. Nishino, J. Arey and R. Atkinson, Products of the OH radical-initiated reactions of furan, 2- and 3-methylfuran, and 2,3- and 2,5-dimethylfuran in the presence of NO, *J. Phys. Chem.*, 2014, **118**, 457–466.

9 J. Jiang, W. P. L. Carter, D. R. Cocker and K. C. Barsanti, Development and evaluation of a detailed mechanism for gas-phase atmospheric reactions of furans, *ACS Earth Space Chem.*, 2020, **4**, 1254–1268.

10 A. Bierbach, I. Barnes and K. H. Becker, Product and kinetic study of the OH-initiated gas-phase oxidation of furan, 2-methylfuran and furanaldehydes at ~300K, *Atmos. Environ.*, 1995, **29**, 2651–2660.

11 E. R. Stephens, The formation, reactions, and properties of peroxyacyl nitrates (PANs) in photochemical air pollution, *Adv. Environ. Sci. Technol.*, 1969, **1**, 119–146.

12 A. P. Altshuller, PANs in the atmosphere, *J. Air Waste Manage. Assoc.*, 1993, **43**, 1221–1230.

13 J. M. Roberts, The atmospheric chemistry of organic nitrates, *Atmos. Environ.*, 1990, **24A**, 243–287.

14 M. J. Newland, Y. Ren, M. R. McGillen, L. Michelat, V. Daële and A. Mellouki, NO_3 chemistry of wildfire emissions: a kinetic study of the gas-phase reactions of furans with the NO_3 radical, *Atmos. Chem. Phys.*, 2022, **22**, 1761–1772.

15 H. B. Singh, Reactive nitrogen in the troposphere, *Environ. Sci. Technol.*, 1987, **21**, 320–327.

16 J. Williams, J. M. Roberts, F. C. Fehsenfeld, S. B. Bertman, M. P. Buhr, P. D. Goldan, G. Hübler, W. C. Kuster, T. B. Ryerson, M. Trainer and V. Young, Regional ozone from biogenic hydrocarbons deduced from airborne measurements of PAN, PPN, and MPAN, *Geophys. Res. Lett.*, 1997, **24**, 1099–1102.

17 J. M. Roberts, F. Flocke, A. Weinheimer, H. Tanimoto, B. T. Jobson, D. Riemer, E. C. Apel, E. Atlas, S. G. Donnelly, V. F. Stroud, K. Johnson, R. Weaver and F. C. Fehsenfeld, Observations of APAN during TexAQS 2000, *Geophys. Res. Lett.*, 2001, **28**, 4195–4198.

18 Y. Lee, L. G. Huey, Y. Wang, H. Qu, R. Zhang, Y. Ji, D. J. TAnner, X. Wang, J. Tang, W. Song, W. Hu and Y. Zhang, Photochemistry of volatile organic compounds in the Yellow River Delta, China: formation of O_3 and peroxyacyl nitrates, *J. Geophys. Res.: Atmos.*, 2021, **126**, e2021JD035296.

19 J. M. Roberts, in *Volatile Organic Compounds in the Atmosphere*, ed. R. Koppmann, Blackwell, London, 2007, pp. 221–268.

20 F. Kirchner, A. Mayer-Figge, F. Zabel and K. H. Becker, Thermal stability of peroxynitrates, *Int. J. Chem. Kinet.*, 1999, **31**, 127–144.

21 M. Kabir, S. Jagiella and F. Zabel, Thermal stability of n-acyl peroxynitrates, *Int. J. Chem. Kinet.*, 2014, **46**, 462–469.

22 J. M. Roberts, M. Marchewka, S. B. Bertman, R. Sommariva, C. Warneke, J. de Gouw, W. Kuster, P. Goldan, E. Williams, B. M. Lerner, P. Murphy and F. C. Fehsenfeld, Measurements of PANs during the New England Air Quality Study, 2002, *J. Geophys. Res.: Atmos.*, 2007, **112**, D20306, DOI: 10.1029/2007JD008667.

23 R. K. Talukdar, J. B. Burkholder, A.-M. Schmoltner, J. M. Roberts, R. R. Wilson and A. R. Ravishankara, Investigation of the loss processes for peroxyacetyl nitrate in the atmosphere: UV photolysis and reaction with OH, *J. Geophys. Res.*, 1995, **100**, 14163–14173.

24 M. H. Harwood, J. M. Roberts, G. J. Frost, A. R. Ravishankara and J. B. Burkholder, Photochemical studies of $CH_3C(O)OONO_2$ (PAN) and $CH_3CH_2C(O)OONO_2$ (PPN): NO_3 quantum yields, *J. Phys. Chem. A*, 2003, **107**, 1148–1154.

25 J. J. Orlando, G. S. Tyndall, S. B. Bertman, W. Chen and J. B. Burkholder, Rate coefficient for the reaction of OH with $CH_2{=}C(CH_3)C(O)OONO_2$ (MPAN), *Atmos. Environ.*, 2002, **36**, 1895–1900.

26 J. J. Orlando and G. S. Tyndall, Mechanisms for the reactions of OH with two unsaturated aldehydes: Crotonaldehyde and acrolein, *J. Phys. Chem. A*, 2002, **106**, 12252–12259.

27 J. Kames and U. Schurath, Henry's law and hydrolysis-rate constants for peroxyacetyl nitrates (PANs) using a homogeneous gas-phase source, *J. Atmos. Chem.*, 1995, **21**, 151–164.

28 J. Kames, S. Schweighoefer and U. Schurath, Henry's law constant and hydrolysis of peroxyacetyl nitrate (PAN), *J. Atmos. Chem.*, 1991, **12**, 169–180.

29 M. W. Holdren, C. W. Spicer and J. M. Hales, Peroxyacetyl nitrate solubility and decomposition rate in acidic water, *Atmos. Environ.*, 1984, **18**, 1171–1173.

30 J. M. Roberts, Measurement of the Henry's law coefficient and the first order loss rate of PAN in n-octanol, *Geophys. Res. Lett.*, 2005, **31**, L08803.

31 S. B. Bertman and J. M. Roberts, A PAN analog from isoprene photooxidation, *Geophys. Res. Lett.*, 1991, **18**, 1461–1464.

32 H. Tanimoto and H. Akimoto, A new peroxycarboxylic nitric anhydride identified in the atmosphere: $CH_2{=}CHC(O)OONO_2$ (APAN), *Geophys. Res. Lett.*, 2001, **28**, 2831–2834.

33 N. D. Rider, Y. M. Taha, C. A. Odame-Ankrah, J. A. Huo, T. W. Tokarek, E. Cairns, S. G. Mouss, J. Liggio and H. D. Osthoff, Efficient photochemical generation of peroxycarboxylic nitric anhydrides with ultraviolet light-emitting diodes, *Atmos. Meas. Tech.*, 2015, **8**, 2737–2748.

34 P. R. Veres and J. M. Roberts, Development of a photochemical source for the production and calibration of acyl peroxynitrate compounds, *Atmos. Meas. Tech.*, 2015, **8**, 2225–2231.

35 P. Warneck and T. Zerbach, Synthesis of peroxyacetyl nitrate in air by acetone photolysis, *Environ. Sci. Technol.*, 1992, **26**, 74–79.

36 A. Volz-Thomas, I. Xueref and R. Schmitt, Automatic gas chromatograph and calibration system for ambient measurements of PAN and PPN, *Environ. Sci. Pollut. Res.*, 2002, **9**, 72–76.

37 H. Niki, P. D. Maker, C. M. Svage and L. P. Breitenbach, An FTIR study of the reactions Br + CH_3CHO -> HBr + CH_3CO and $CH_3C(O)OO$ + NO_2 -> $CH_3C(O)OONO_2$ (PAN), *Int. J. Chem. Kinet.*, 1985, **17**, 525–534.

38 J. Williams, J. M. Roberts, S. B. Bertman, C. A. Stroud, F. C. Fehsenfeld, K. Baumann, M. P. Buhr, K. Knapp, P. C. Murphy, M. Nowick and E. J. Williams, A method for the airborne measurement of PAN, PPN, and MPAN, *J. Geophys. Res.*, 2000, **105**, 28943–28960.

39 J. M. Roberts, P. Veres, C. Warneke, J. A. Neuman, R. A. Washenfelder, S. S. Brown, M. Baasandorj, J. B. Burkholder, I. R. Burling, T. J. Johnson, R. J. Yokelson and J. de Gouw, Measurement of HONO, HNCO, and other inorganic acids by negative-ion proton-transfer chemical-ionization mass spectrometry (NI-PT-CIMS): application to biomass burning emissions, *Atmos. Meas. Tech.*, 2010, **3**, 981–990.

40 P. R. Veres, J. A. Neuman, T. H. Bertram, E. Assaf, G. M. Wolfe, C. J. WIlliamson, B. Weinzierl, S. Tilmes, C. Thompson, A. B. Thames, J. C. Schroder, A. Saiz-Lopez, A. W. Rollins, J. M. Roberts, D. Price, J. Peischl, B. A. Nault, K. H. Møller, D. O. MIller, S. Meinardi, Q. Li, J.-F. Lamarque, A. Kupc, H. G. Kjaergaard, D. Kinnison, J. L. Jimenez, C. M. Jernigan, R. S. Hornbrook, A. Hills, M. Dollner, D. A. Day, C. A. Cuevas, P. Campuzano-Jost, J. B. Burkholder, T. P. Bui, W. H. Brune, S. S. Brown, C. A. Brock, I. Bourgeois, D. R. Blake, E. C. Apel and T. B. Ryerson, In-situ observations reveal the importance of dimethyl sulfide autoxidation in the marine atmosphere, *Proc. Natl. Acad. Sci. U. S. A.*, 2020, **117**, 4505–4510.

41 C. Warneke, M. T. Trainer, J. A. de Gouw, D. D. Parrish, D. W. Fahey, A. R. Ravishankara, A. M. Middlebrook, C. A. Brock, J. M. Roberts, S. S. Brown, J. A. Neuman, B. M. Lerner, D. Lack, D. Law, G. Huebler, I. Pollack, S. Sjostedt, T. B. Ryerson, J. A. Gilman, J. Liao, J. Holloway, J. Peischl, J. B. Nowak, K. Aikin, K.-E. Min, R. A. Washenfelder, M. Graus, M. Richardson, M. Z. Markovic, N. L. Wagner, A. Welti, P. R. Veres, P. Edwards, J. P. Schwarz, T. Gordon, W. P. Dube, S. A. McKeen, J. Brioude, R. Ahmadov, A. Bougiatioti, J. J. Lin, A. Nenes, G. M. Wolfe, T. F. Hanisco, B. H. Lee, F. D. Lopez-Hilfiker, J. A. Thornton, F. N. Keutsch, J. Kaiser, J. Mao and C. D. Hatch, Instrumentation and measurement strategy for the NOAA SENEX aircraft campaign as part of the Southeast Atmosphere Study 2013, *Atmos. Meas. Tech.*, 2016, **9**, 3063–3093.

42 W. Zheng, F. M. Flocke, G. S. Tyndall, A. Swanson, J. J. Orlando, J. M. Roberts, L. G. Huey and D. J. Tanner, Characterization of a thermal dissociation chemical ionization mass spectrometer for the measurement of peroxy acyl nitrates (PANs) in the atmosphere, *Atmos. Chem. Phys.*, 2011, **11**, 6529–6547.

43 D. L. Slusher, L. G. Huey, D. J. Tanner, F. M. Flocke and J. M. Roberts, A thermal dissociation-chemical ionization mass spectrometry (TD-CIMS) technique for the simultaneous measurement of peroxyacyl nitrates and dinitrogen pentoxide, *J. Geophys. Res.: Atmos.*, 2004, **109**, D19315, DOI: **10.1029/2004JD004670**.

44 M. Breitenlechner, G. A. Novak, J. A. Neuman, A. W. Rollins and P. R. Veres, A versatile vacuum ultraviolet ion source for reduced pressure bipolar chemical ionization mass spectrometry, *Atmos. Meas. Tech.*, 2022, **15**, 1159–1169.

45 T. B. Ryerson, A. E. Andrews, W. M. Angevine, T. S. Bates, C. A. Brock, B. Cairns, R. C. Cohen, O. R. Cooper, J. A. de Gouw, F. C. Fehsenfeld, R. A. Ferrare, M. L. Fischer, R. C. Flagan, A. H. Goldstein, J. W. Hair, R. M. Hardesty, C. A. Hostetler, J. L. Jimenez, A. O. Langford, E. McCauley, S. A. McKeen, L. T. Molina, A. Nenes, S. J. Oltmans, D. D. Parrish, J. R. Pederson, R. B. Pierce, K. Prather, P. K. Quinn, J. H. Seinfeld, C. J. Senff, A. Sorooshian, J. Stutz, J. D. Surratt, M. Trainer, R. Volkamer, E. J. Williams and S. C. Wofsy, The 2010 California Research at the Nexus of Air Quality and Climate Change (CalNex) field study, *J. Geophys. Res.: Atmos.*, 2013, **118**, 5830–5866.

46 B. Yuan, A. R. Koss, C. Warneke, J. B. Gilman, B. M. Lerner, H. Stark and J. A. de Gouw, A high-resolution time-of-flight chemical ionization mass spectrometer utilizing hydronium ions (H_3O^+ ToF-CIMS) for measurements of volatile organic compounds in the atmosphere, *Atmos. Meas. Tech.*, 2016, **9**, 2735–2752.

47 S. J. Eilerman, J. Peischl, J. A. Neuman, T. B. Ryerson, K. C. Aikin, M. W. Holloway, M. A. Zondlo, L. M. Golston, D. Pan, C. Floechinger and S. Herndon, Characterization of ammonia, methane, and nitrous oxide emissions from concentrated animal feeding operations in Northeastern Colorado, *Environ. Sci. Technol.*, 2016, **50**, 10885–10893.

48 B. D. Hall, G. S. Dutton and J. W. Elkins, The NOAA nitrous oxide standard scale for atmospheric observations, *J. Geophys. Res.: Atmos.*, 2007, **112**, D09305.

49 J. M. Roberts and Y. Liu, Solubility and solution-phase chemistry of isocyanic acid, methyl isocyanate and cyanogen halides, *Atmos. Chem. Phys.*, 2019, **19**, 4419–4437.

50 G. J. Phillips, N. Pouvesle, J. Thieser, G. Schuster, R. Axinte, H. Fischer, J. Williams, J. Lelieveld and J. N. Crowley, Peroxyacetyl nitrate (PAN) and peroxyacetic acid (PAA) measurements by iodide chemical ionisation mass spectrometry: First analysis of results in the boreal forest

and implications for the measurement of PAN fluxes, *Atmos. Chem. Phys.*, 2013, **13**, 1129–1139.

51 L. H. Mielke and H. D. Osthoff, On quantitative measurements of peroxycarboxylic nitric anhydride mixing ratios by thermal dissociation chemical ionization mass spectrometry, *Int. J. Mass Spectrom.*, 2012, **310**, 1–9.

52 M. A. Robinson, J. A. Neuman, L. G. Huey, J. M. Roberts, S. S. Brown and P. R. Veres, Temperature dependent sensitivity of iodide chemical ionization mass spectrometers, *Atmos. Meas. Tech.*, 2022, DOI: **10.5194/amt-2022-295**.

53 C. M. Strollo and P. J. Ziemann, Products and mechanism of secondary organic aerosol formation from the reaction of 3-methylfuran with OH radicals in the presence of NOx, *Atmos. Environ.*, 2013, **77**, 534–543.

54 J. D. Crounse, L. B. Nielsen, S. Jørgensen, H. G. Kjaergaard and P. O. Wennberg, Autooxidation of organic compounds in the atmosphere, *J. Phys. Chem. Lett.*, 2013, **4**, 3513–3520.

55 NOAA Chemical Sciences Laboratory, *SUNVEx/RECAP Pasadena Data Archive*, **https://csl.noaa.gov/groups/csl7/measurements/2021sunvex/GroundLA/DataDownload/**, accessed March 3, 2022.

56 I. Bridier, F. Caralp, H. Loirat, B. Veyret, K. H. Becker, A. Reimer and F. Zabel, Kinetic and theoretical studies of the reactions $CH_3C(O)O_2 + NO_2 + M \leftrightarrow CH_3C(O)OONO_2 + M$ between 248 and 393K and between 30 and 760 torr, *J. Phys. Chem.*, 1991, **95**, 3594–3600.

57 J. Troe, Predictive possibilities of unimolecular rate theory, *J. Phys. Chem.*, 1979, **83**, 114–126.

58 R. Sander, Compilation of Henry's law constants (version 4.0) for water as solvent, *Atmos. Chem. Phys.*, 2015, **15**, 4399–4981.

59 T. Raventos-Duran, M. Camredon, R. Valorso, C. Mouchel-Vallon and B. Aumont, Structure-activity relationships to estimate the effective Henry's law constants of organics of atmospheric interest, *Atmos. Chem. Phys.*, 2010, **10**, 7643–7654.

60 R. P. Steer, K. R. Darnall and J. N. Pitts Jr., The base-induced decomposition of peroxyacetylnitrate, *Tetrahedron Lett.*, 1969, **43**, 3765–3767.

61 S. Goldstein, J. Lind and G. Merenyi, Chemistry of peroxynitrites as compared to peroxynitrates, *Chem. Rev.*, 2005, **105**, 2457–2470.

62 A. Leo, C. Hansch and D. Elkins, Partition coefficients and their uses, *Chem. Rev.*, 1971, **71**, 525–616.

63 R. Atkinson, D. L. Baulch, R. A. Cox, J. N. Crowley, R. F. Hampson, R. G. Hynes, M. E. Jenkin, M. J. Rossi and J. Troe, Evaluated kinetic and photochemical data for atmospheric chemistry: volume II - gas phase reactions of organic species, *Atmos. Chem. Phys.*, 2006, **6**, 3625–4055.

64 South Pasadena News, *Local news: fire at Debs Park: LAFD with air support response*, **https://southpasadenan.com/breaking-news-fire-at-debs-park-lafd-with-air-support/**, 2021, accessed April 2022.

65 Z. C. J. Decker, K. J. Zarzana, M. Coggon, K.-E. Min, J. Holloway, I. Pollack, T. B. Ryerson, P. Edwards, W. P. Dube, J. P. Schwarz, M. Z. Markovic, C. A. Brock, J. M. Roberts, P. R. Veres, A. R. Koss, L. E. Hatch, K. C. Barsanti and S. S. Brown, Nighttime chemical transformation in biomass burning plumes: a box model analysis initialized with aircraft observations, *Environ. Sci. Technol.*, 2019, **53**, 2529–2538.

66 T. Funazukuri, R. R. Hudgins and P. L. Silveston, Production of olefins from flash pyrolysis of cellulose-containing material, *J. Anal. Appl. Pyrolysis*, 1989, **17**, 47–66.

67 K. Katō, Pyrolysis of cellulose Part III. Comparative studies of the volatile compounds from pyrolysates of cellulose and its related compounds, *Agric. Biol. Chem.*, 1967, **31**, 657–663.

68 E. Grosjean, D. Grosjean, M. P. Fraser and G. R. Cass, Air quality model evaluation data for organics. 3. Peroxyacetyl nitrate and peroxypropionyl nitrate in Los Angeles air, *Environ. Sci. Technol.*, 1996, **30**, 2704–2714.

69 J. M. Roberts, F. Flocke, C. A. Stroud, D. Hereid, E. J. Williams and F. C. Fehsenfeld, Ground-based measurements of PANs during the 1999 Southern Oxidants Study Nashville intensive, *J. Geophys. Res.: Atmos.*, 2002, **107**, 4554.

70 M. J. Alvarado, J. A. Logan, J. Mao, E. Apel, D. Riemer, D. Blake, R. C. Cohen, K.-E. Min, A. E. Perring, E. C. Browne, P. J. Wooldridge, G. S. Diskin, G. W. Sachse, H. Fuelberg, W. R. Sessions, D. L. Harrington, L. G. Huey, J. Liao, A. Case-Hanks, J. L. Jimenez, M. J. Cubison, S. A. Vay, A. J. Weinheimer, D. J. Knapp, D. D. Montzka, F. M. Flocke, I. B. Pollack, P. O. Wennberg, A. Kurten, J. D. Crounse, J. M. St. Clair, A. Wisthaler, T. Mikoviny, R. M. Yantosca, C. C. Carouge and P. Le Sager, Nitrogen oxides and PAN in plumes from boreal fires during ARCTAS-B and their impact on ozone: an integrated analysis of aircraft and satellite observations, *Atmos. Chem. Phys.*, 2010, **10**, 9739–9760.

71 Y.-N. Lee, in *Gas-Liquid Chemistry of Natural Waters*, Brookhaven National Laboratory, Upton, N.Y., 1984, vol. BNL-51757.

72 X. Liu, Y. Zhang, L. G. Huey, R. J. Yokelson, Y. Wang, J. L. Jimenez, P. Campuzano-Jost, A. J. Beyersdorf, D. R. Blake, Y. Choi, J. M. St. Clair, J. D. Crounse, D. A. Day, G. S. Diskin, A. Fried, S. R. Hall, T. F. Hanisco, L. E. King, S. Meinardi, T. Mikoviny, B. B. Palm, J. Peischl, A. E. Perring, I. B. Pollack, T. B. Ryerson, G. W. Sachse, J. P. Schwarz, I. J. Simpson, D. J. Tanner, K. L. Thornhill, K. Ullman, R. J. Weber, P. O. Wennberg, A. Wisthaler, G. M. Wolfe and L. D. Ziemba, Agricultural fires in the southeastern U.S. during SEAC^{4}RS: emissions of trace gases and particles and evolution of ozone, reactive nitrogen, and organic aerosol, *J. Geophys. Res.: Atmos.*, 2016, **121**, 7383–7414.

73 J. M. Roberts, C. A. Stroud, B. T. Jobson, M. Trainer, D. Hereid, E. J. Williams, F. C. Fehsenfeld, W. H. Brune, M. Martinez and H. Harder, Application of a sequential reaction model to PANs and aldehyde measurements in two urban areas, *Geophys. Res. Lett.*, 2001, **28**, 4583–4586.